Crystal Research and Technology

CRYSTAL Research & Technology

www.crt-journal.org

RESEARCH ARTICLE

Microwave-Assisted Synthesis of Tunable CuO Nanostructures for Photocatalytic Detoxification of Eosin Yellow Dye

Govindan Suresh Kumar[1] | Kesavan Lalithambigai[2] | Selvaraj Ranjith Priyan[3] | Srinivasan Ramalingam[4] | Raji Atchudan[5,6] | Mohd. Shkir[7,8,9]

[1]Department of Physics, PSG College of Arts & Science, Coimbatore, Tamil Nadu 641014, India | [2]Department of Physics, K.S.R. College of Engineering, Namakkal, Tamil Nadu 637215, India | [3]Department of Physics, K.S. Rangasamy College of Arts and Science (Autonomous), Namakkal, Tamil Nadu 637215, India | [4]Department of Horticulture and Life Science, Yeungnam University, Gyeongsan, Gyeongsangbuk-do 38541, Republic of Korea | [5]Department of Chemistry, Saveetha School of Engineering, Saveetha Institute of Medical and Technical Sciences, Chennai, Tamil Nadu 602105, India | [6]School of Chemical Engineering, Yeungnam University, Gyeongsan, Gyeongsangbuk-do 38541, Republic of Korea | [7]Department of Physics, College of Science, King Khalid University, PO Box 960, AlQura'a, Abha61421, Saudi Arabia | [8]Smart Nano-Materials for Energy and Optoelectronic Devices Lab, Central Labs, King Khalid University, PO Box 960, AlQura'a, Abha61421, Saudi Arabia | [9]University Center for Research & Development, Chandigarh University, Gharuan, Mohali, Punjab 140413, India

Correspondence: Govindan Suresh Kumar (gsureshkumar1986@gmail.com) | Srinivasan Ramalingam (sribt27@gmail.com) | Raji Atchudan (atchudanr@yu.ac.kr)

Received: 11 May 2025 | **Revised:** 21 November 2025 | **Accepted:** 26 November 2025

Keywords: CuO nanostructures | microwave-assisted synthesis | morphology | photocatalysis | wastewater treatment

ABSTRACT

In this study, we report the microwave-assisted synthesis of morphology-controlled cupric oxide (CuO) nanostructures using ethylenediaminetetraacetic acid (EDTA) and polyethylene glycol (PEG) as morphology-controlling agents. The structural, morphological, and optical properties of the prepared CuO nanostructures are thoroughly investigated using XRD, FTIR, FESEM, EDX, PL, and UV–vis spectroscopy. XRD analysis revealed the development of monoclinic CuO with different crystallinity. FESEM analysis showed that the CuO synthesized in the absence of an organic modifier exhibited a flake-like nanostructure, whereas the use of PEG and EDTA as morphology controllers resulted in the formation of spherical and rod-like nanostructures, respectively. The photocatalytic test was conducted on eosin yellow dye degradation using the synthesized CuO nanostructures under visible light for 120 min. The shape-dependent photocatalytic degradation of eosin yellow dye by the synthesized CuO nanostructures was observed with the respective degradation efficiencies of 81.70%, 95.50%, and 98.13% for flake-like, spherical, and rod-like nanostructures. Hence, morphology-controlled synthesis plays a key role in optimizing the photocatalytic performance of CuO nanostructures, making them more effective for environmental remediation.

1 | Introduction

In recent decades, materials research has increasingly focused on nanoscale materials, which are emerging as powerful tools for addressing environmental pollution. Nanoscale materials exhibit unique physicochemical characteristics compared to their bulk counterparts, owing to quantum confinement effects and a high surface area [1, 2]. The properties of nanostructures can be engineered for energy, environment, and healthcare applications, as they tend to depend more on their size and morphology [1, 3]. Nanostructured cupric oxide (CuO) has been among the nanomaterials that have attracted considerable attention

due to its wide range of applications, including solar cells, batteries, supercapacitors, photodetectors, sensors, and photocatalysis, among others. CuO is the p-type transition metal oxide semiconductor with a narrow bandgap of 1.2 eV when in bulk. CuO has a monoclinic crystal structure with C2/c symmetry [4–6]. The photocatalytic reactivity of CuO nanostructures is significantly influenced by their size, shape, and crystallographic orientation [5, 6]. Thus, it is essential to modify the synthesis techniques, which can lead to the design of CuO nanostructures with controlled dimensions, shapes, and specific crystallographic directions, thereby enabling photocatalytic activity toward the degradation of organic pollutants [6–8].

Nanostructured CuO can be prepared through various chemical and physical techniques, including hydrothermal, sol–gel, solvothermal, and chemical vapor deposition [5, 6]. All these methods have their specific merits; however, long reaction times, very high temperatures, and expensive precursors hinder them from being practical or scalable for industrial applications. In this context, microwave-assisted synthesis has established itself as a promising method for developing nanomaterials with tunable morphologies due to its rapid energy efficiency and cost-effectiveness [9, 10]. Microwave irradiation can provide heat evenly and simultaneously, thereby contributing to higher reaction rates and the formation of nanostructures with tunable shapes and sizes [11, 12]. Microwave irradiation appears to be a promising method to rapidly and efficiently synthesize a variety of advanced materials, particularly in biomedical engineering, catalysis, and energy storage. Unlike conventional thermal methods, which rely on conduction and convection to transfer heat from the outer surface to the interior of the material, microwave irradiation enables volumetric heating through the direct coupling of microwave energy with polar molecules and ionic species present in the reaction mixture. The typical microwave heating frequency is 2.45 GHz. The microwave heating mechanism is primarily based on two well-known phenomena: the first is dipolar polarization, in which polar molecules align themselves according to the rapidly alternating electric field, thereby producing heat due to intermolecular friction. The second one is ionic conduction, in which dissolved ions move due to the electric field, colliding with surrounding molecules and producing heat. The combined effect causes a very high local temperature, providing tremendous acceleration to reaction kinetics, nucleation rates, and crystal growth [11, 12]. Thus, this technique allows for the synthesis of morphology-controlled CuO nanostructures within a shorter duration.

One of the most promising prospects for CuO nanostructures is their capability as photocatalysts for degrading organic contaminants in wastewater [5]. The discharge of toxic organic chemicals through industrial processes into water bodies poses a significant threat to both the environment and human health, prompting extensive research on the development of efficient and sustainable remediation technologies [13–15]. Photocatalytic degradation of organic contaminants using semiconductor materials activated by either UV or visible light has attracted significant interest as a sustainable technique [15–18]. In this context, the advantages of CuO nanostructures include their high absorption in the visible light region, ease of preparation, and ecological compatibility, which are considerable [5, 6, 19]. However, the photocatalytic activity of CuO is highly dependent on its morphological or even surface characteristics. Therefore, it is necessary to control and shape the structures of CuO nanomaterials to improve their photocatalytic efficiency for degrading organic pollutants [5, 20].

In this work, we present a facile method for synthesizing CuO nanostructures of controlled morphologies using microwave-assisted techniques and their application in the photodegradation of organic pollutant. Microwave-assisted techniques offer a rapid and straightforward process for synthesizing CuO nanostructures with tunable morphologies, including nanorods, nanospheres, and nanoflakes [9–12]. This can be achieved by optimizing reaction conditions, such as precursor concentration, reaction time, and microwave power, which tailor the size, shape, and crystallinity of the unfolded nanostructures [10, 11]. This is also very important for enhancing photocatalytic activities of emerging nanomaterials, as the surface area and exposed crystal facets significantly affect their reactivity [21].

The primary objective of this research is to develop an efficient and facile method for synthesizing CuO nanostructures with designed morphologies and to investigate their photocatalytic application for the degradation of organic pollutants, such as dyes and pharmaceuticals, under visible-spectrum irradiation. Tailoring the morphologies of CuO nanostructures thus provides an opportunity to optimize their photocatalytic performance, making them of intense interest in wastewater treatment applications [5, 7, 22]. Hence, the current research focuses on developing a microwave-assisted synthetic route for the preparation of CuO nanostructures in a controlled morphological form. Another part of the study also aims to evaluate the photocatalytic activity of the synthesized CuO nanostructures in removing organic pollutants under visible light irradiation. It can thus contribute toward developing a sustainable and efficient solution for the synthesis of morphology-controlled CuO nanostructures. This research, therefore, has important implications for environmental remediation and wastewater treatment technologies.

2 | Experimental Procedure

2.1 | Materials

The materials used were copper(II) nitrate trihydrate ($Cu(NO_3)_2{\cdot}3H_2O$, purity ≥ 99%, Merck, India,) as the copper source, ethylenediaminetetraacetic acid (EDTA, $C_{10}H_{16}N_2O_8$, purity ≥ 99%, Merck, India,) and polyethylene glycol ($H{-}(O{-}CH_2{-}CH_2)_n{-}OH$, PEG, molecular weight: 3350, purity≥98%, HiMedia Laboratories Pvt. Ltd.) as chelating agents to control nanoparticle morphology, sodium hydroxide (NaOH, purity∼97%, Nice Chemicals Pvt. Ltd.) as the precipitating agent, deionized water as the solvent, and eosin yellow ($C_{20}H_8Br_4O_5$, purity∼90%, Loba Chemie, Pvt. Ltd) as a model pollutant for photodegradation studies.

2.2 | Synthesis of CuO Nanostructure with Different Morphologies

The cupric oxide (CuO) nanostructures with different sizes and shapes were synthesized using a microwave-assisted method using EDTA or PEG as chelating agents [23, 24]. An aqueous

solution of 0.1 M $Cu(NO_3)_2 \cdot 3H_2O$ was prepared in 100 mL of distilled water as the copper source, to which an EDTA or PEG solution was added dropwise under continuous stirring. The resulting mixture was refluxed for 1 h to obtain a homogeneous solution. Then, 40 mL of 0.1 M sodium hydroxide was gradually added to adjust the pH to 11 with vigorous stirring. The obtained mixture was then placed in a microwave oven (Make: LG Electronics India Pvt. Ltd.) and subjected to microwave irradiation for 10 min at 700 W. After microwave treatment, the solution was allowed to cool to ambient temperature, and the precipitated CuO nanostructures were collected by centrifugation. The collected precipitate was systematically washed with distilled water, followed by ethanol, to remove impurities, and thendried at 110°C to obtain the CuO product. The samples were prepared with the addition of EDTA or PEG as chelating agents, respectively. Additionally, pure CuO was prepared without the use of chelating agents using the above procedure for comparison.

2.3 | Characterization

The prepared CuO nanostructures were analyzed in detail for their structural, morphological, elemental, and optical properties. The X-ray powder diffraction (XRD) analysis was carried out using a Bruker D8 Advance X-ray diffractometer with a Cu Kα radiation source (λ = 1.5406 Å) covering an angular range of 2θ between 20° and 80°. The voltage and current settings were 40 kV and 40 mA for operation, respectively. The indexing of resultant diffraction peaks was done using JCPDS standard data (Card No. 05–0661) To identify functional groups and verify the chemical bonding in CuO nanostructures, Fourier Transform Infrared (FTIR) spectroscopy was used for examination. FTIR spectra were obtained in the mid-infrared range of (4000–400 cm) with a Bruker Tensor 27 spectrometer. For this process, samples were prepared by homogeneously mixing the CuO powder with spectroscopic-grade potassium bromide (KBr) at a ratio of 1:100 and pressing the mixture into pellets using a hydraulic pellet press. FESEM analysis was employed to examine the surface morphology and particle size of the CuO nanostructures. Imaging was performed on the Carl Zeiss Sigma 300 FESEM. All samples were preliminarily sputter-coated with a thin layer of gold to improve conductivity. Elemental composition and purity were assessed using Energy Dispersive X-ray Spectroscopy (EDX) attached to a Carl Zeiss Sigma 300 FESEM. The photoluminescence (PL) spectrum of the samples was recorded using a Shimadzu RF-5301 PC spectrofluorophotometer in the range of 300–500 nm with excitation wavelength 325 nm. The UV-vis-NIR diffuse reflectance spectra of the samples were measured on a Shimadzu UV-2600 spectrophotometer in the wavelength range of 200–1400 nm.

2.4 | Eosin Yellow Dye Degradation Tests

Eosin yellow is a model organic pollutant that is most commonly used in photocatalytic degradation studies. Eosin yellow is a commercially utilized xanthene dye in various industries, including imaging, textiles, paper, and cosmetics [25]. The photocatalytic degradation of eosin yellow dye was studied using 100 mg of synthesized photocatalyst, mixed with 100 mL of a 50 mg/L eosin yellow dye solution, and illuminated with UV light for 120 min. This mixture was stirred under dark conditions for 1 h to allow it to establish an adsorption–desorption equilibrium before exposure to UV light. The degradation of eosin yellow dye was observed by measuring the difference in absorbance at its characteristic wavelength (517 nm) using a UV–vis spectrophotometer. The efficiency of dye degradation was determined by comparing absorbance values before and after exposure to light over a set time [22, 26].

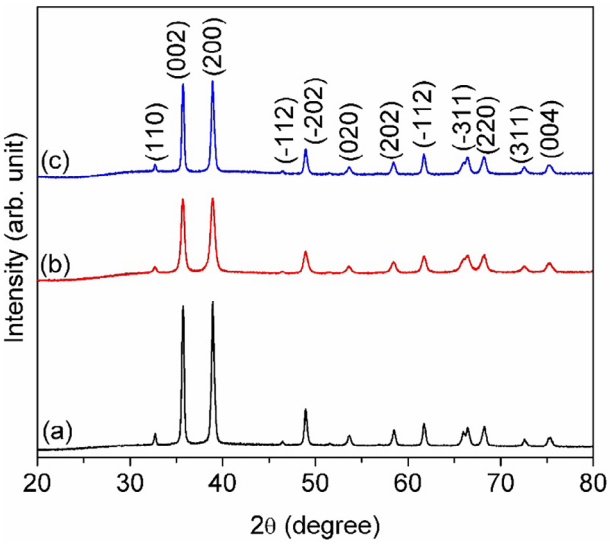

FIGURE 1 | XRD pattern of CuO nanostructures synthesized via the microwave method (a) without a chelating agent, (b) with EDTA, and (c) with PEG.

3 | Results and Discussion

The XRD patterns of the synthesized CuO are revealed in Figure 1. All XRD patterns show clear diffraction peaks at 32.5°, 35.5°, 38.7°, 48.7°, 53.4°, 58.3°, 61.5°, 66.3°, 68.1°, 72.4°, and 75.2°. All these peaks can be indexed to the monoclinic phase of CuO, which matches well with the standard JCPDS card number. 45–0937. The diffraction peaks observed in Figure 1b,c were much broader and less intense than the corresponding peaks obtained for the sample synthesized without a chelating agent (Figure 1a). This suggests that the chelating agent-assisted CuO samples may have lower crystallinity and possibly smaller crystallite sizes. On the other hand, these results showed that the chelating agents stabilize the copper ions and control the growth of the crystal, yielding CuO of a lower degree of crystallinity and possibly smaller crystallite sizes. From this analysis, it is clear that chelating agents, i.e., EDTA and PEG, have a significant effect on tuning the crystallinity and structural quality of CuO. Madona et al. observed that surfactants influence the intensity of diffraction peaks in CuO nanostructures [27], which aligns well with our results. The calculated lattice parameters shown in Table 1 also indicate that chelating agents alter the lattice parameters of the monoclinic unit cell of the CuO sample. It suggests that the lattice constants of CuO samples are influenced by chelating agents, which reflects internal structural effects. The slight variations in the unit cell dimensions due to EDTA are evidence of minor structural changes. In contrast, PEG demonstrates a much more pronounced expansion of the lattice,

TABLE 1 | Lattice constant and cell volume of the CuO samples prepared without and with chelating agents.

Sample code	Chelating agent	Lattice constant and cell volume			
		a **(Å)**	***b*** **(Å)**	***c*** **(Å)**	***V*** **(Å^3)**
CO	Nil	4.8557	3.2942	4.4794	71.46
ECO	EDTA	4.8520	3.2979	4.4818	71.52
PCO	PEG	4.8586	3.2981	4.4804	71.61

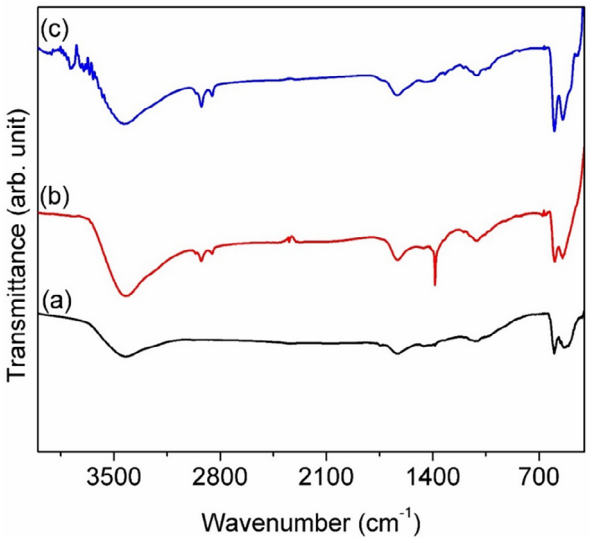

FIGURE 2 | FTIR spectrum of CuO nanostructures synthesized via the microwave method. (a) without a chelating agent, (b) with EDTA, and (c) PEG.

indicating stronger molecular interactions during synthesis. It suggests that chelation influences the lattice and crystal structure, which could ultimately impact the electronic properties, defect density, and performance of the material in different applications.

The FTIR spectrum of CuO nanostructures synthesized via the microwave method, with and without a chelating agent, is shown in Figure 2, revealing the vibrations of different functional groups present in the samples. The entire spectrum exhibits prominent peaks in the range of 500–600 cm^{-1}, indicating the Cu—O vibration, which confirms the formation of CuO [28, 29]. Furthermore, a broad band around 3500 cm^{-1} and a peak at 1632 cm^{-1} were observed in all samples, corresponding to the vibrations of hydroxyl groups due to surface-bounded water molecules [30]. The spectra also show peaks in the region of 2850–2950 cm^{-1}, associated with C-H stretching vibrations, which are most prominent in the samples synthesized using EDTA and PEG, implying the presence of organic residues from these chelating agents [30–32]. The peaks seen at 1386 cm^{-1} and at 1450 cm^{-1} are attributed to carboxylate COO- stretch vibrations, likely introduced by the residual organic molecules present during the synthesis [27, 31]. The peaks observed around 1055 and 1124 cm^{-1} were due to C—H bend vibrations, thus confirming the interaction of organic moieties with the CuO surface [30–33]. The observed variations in peak intensity and wavenumber shifts among the three spectra serve as evidence that EDTA and PEG have played a modifying role on the surface chemistry of CuO nanostructures [33, 34]. The presence of chelating agents would likely modulate the adsorption of organic residues and thus create a defect or modify the electronic structure of the material. Such changes could have a profound impact on the functional properties of CuO, particularly its photocatalytic ability.

Figure 3 depicts the FESEM images of the CuO nanostructures synthesized via the microwave method under varying conditions: without a chelating agent, with EDTA, and with PEG. The CuO nanostructure synthesized without a chelating agent, as revealed in Figure 3a–c, exhibits irregular, flaky, and plate-like structures with rough surfaces and poor uniformity in shape and size, with individual flakes measuring several hundred nanometers across. The CuO with irregular, flaky, and plate-like structures was formed as follows: When the copper nitrate aqueous solution was added with NaOH, copper hydroxide ($Cu(OH)_2$) precipitates were formed. This mixture was then subjected to microwave irradiation, where $Cu(OH)_2$ decomposed quickly into CuO and water due to rapid heating [35]. The extremely rapid thermal decomposition gives rise to many CuO nuclei almost instantaneously. The microwaves provide such high energy that they ensure uniform but speedy decomposition, resulting in different nucleation and growth rates in various regions of the solution, thus forming irregular CuO particles. The fast-growing nuclei are conducive to the development of flaky and platey structures as the particles tend to aggregate and, under the influence of rapidly varying thermal conditions, orient in specific directions. Moreover, NaOH affects the pH of the medium, which also affects the solubility and growth of CuO particles. High pH values contribute to the formation of more CuO nuclei, but a faster heating rate could lead to an uncontrolled growth pathway, resulting in rougher surfaces and poor uniformity. Bajaj et al. have prepared CuO nanoflakes via microwave-assisted synthesis without the use of any chelating agents, which strongly corroborates our results [36].

On the other hand, Figure 3d–f showed that when EDTA was added, spherical particles were formed, which were rather homogeneous in size, approximately 10–20 nm in diameter. The uniform CuO nanoparticles with a spherical shape were formed in the presence of EDTA as follows. EDTA is a complexing agent that forms a stable complex with metal ions [33]. Hence, Cu^{2+} ions can be reacted with EDTA and form a stable Cu-EDTA complex, which controls the release of Cu^{2+} ions. When sodium hydroxide is added, hydroxide ions (OH^-) will react with the Cu^{2+} ions, precipitating a copper hydroxide ($Cu(OH)_2$), which is then subjected to microwave irradiation. The microwave irradiation provides rapid and uniform heating, which accelerates the reaction and promotes homogeneous nucleation. During this process, the $Cu(OH)_2$ loses water and converts into CuO nanoparticles. EDTA is crucial in this process as it controls

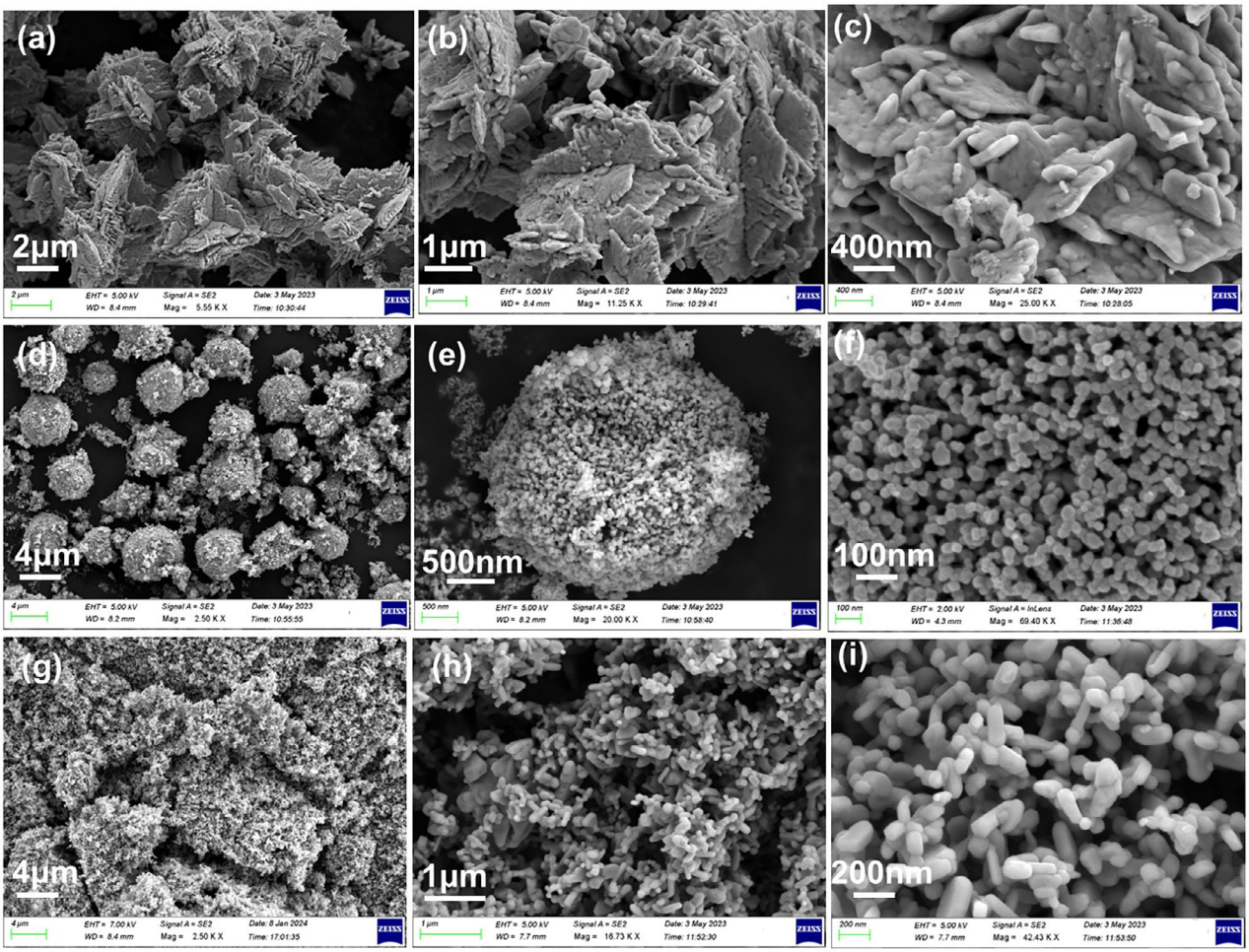

FIGURE 3 | FESEM images of CuO nanostructures synthesized via the microwave method (a–c) without a chelating agent, (d–f) with EDTA, and (g–i) PEG.

the release of ions and keeps them apart, thereby ensuring a spherical and uniform CuO. Figure 3g–i reveals that the use of PEG as a chelating agent resulted in CuO nanostructures showing rod-like or elongated features at higher magnifications. The individual rod-like structures are approximately 100–200 nm long and 40–50 nm thick. Copper nitrate reacts with NaOH to form copper hydroxide, with PEG stabilizing the copper ions by chelation. Microwave irradiation then provides rapid and uniform heating, decomposing the copper hydroxide into CuO. PEG molecules preferentially adsorb on specific crystal facets, directing growth into rod-like structures by inhibiting growth in particular directions [34, 37]. These results clearly revealed the role of chelating agents in determining the morphology and size of CuO nanostructures during microwave synthesis.

The EDS spectra, elemental mapping, and elemental composition analysis are presented in Figure 4. The effect of chelating agents on the Cu to O ratio in CuO nanostructures is evident from the EDS spectra and elemental composition data. Comparing the CuO nanostructures produced in the absence of a chelating agent to those synthesized with EDTA and PEG reveals apparent differences in the copper to oxygen ratio. The EDS spectrum shown in Figure 4a is for the CuO nanostructures synthesized in the absence of a chelating agent. The EDS spectrum shows significant peaks due to copper and oxygen, with weight percentages of 76.70% Cu and 23.30% O, and atomic percentages of 45.32% Cu and 54.68% O. The atomic ratio is about 0.83. Figure 4b shows the EDS spectrum for CuO nanostructures synthesized using EDTA as a chelating agent. EDS spectrum analysis yields weight percentages of 77.47% Cu and 22.53% O, corresponding to atomic percentages of 46.41% Cu and 53.59% O. The atomic ratio is approximately 0.87. The fact that EDTA increases the Cu to O weight ratio suggests that EDTA effectively coordinates copper ions, potentially facilitating copper incorporation into the nanostructure [33]. EDTA can stabilize the copper ions due to its multiple binding sites, leading to more evenly grown CuO nanostructures with a higher relative copper content. In addition, Figure 4c shows the EDS data and elemental mapping for CuO nanostructures prepared using PEG as a chelating agent. EDS data reveal the weight percentages of 78.16% Cu and 21.84% O, atomic percentages of 47.39% Cu and 52.61% O, and an atomic ratio of roughly 0.90. PEG acts as both a stabilizer and a capping agent, which better facilitates the incorporation of copper ions into the nanostructure, thereby offering a larger relative copper content compared to oxygen [34], thereby further enhancing the Cu:O ratio. This indicates that both EDTA and PEG enhance the Cu:O ratio of CuO nanostructures in comparison to the synthesis carried out without chelation. The chelating agents are,

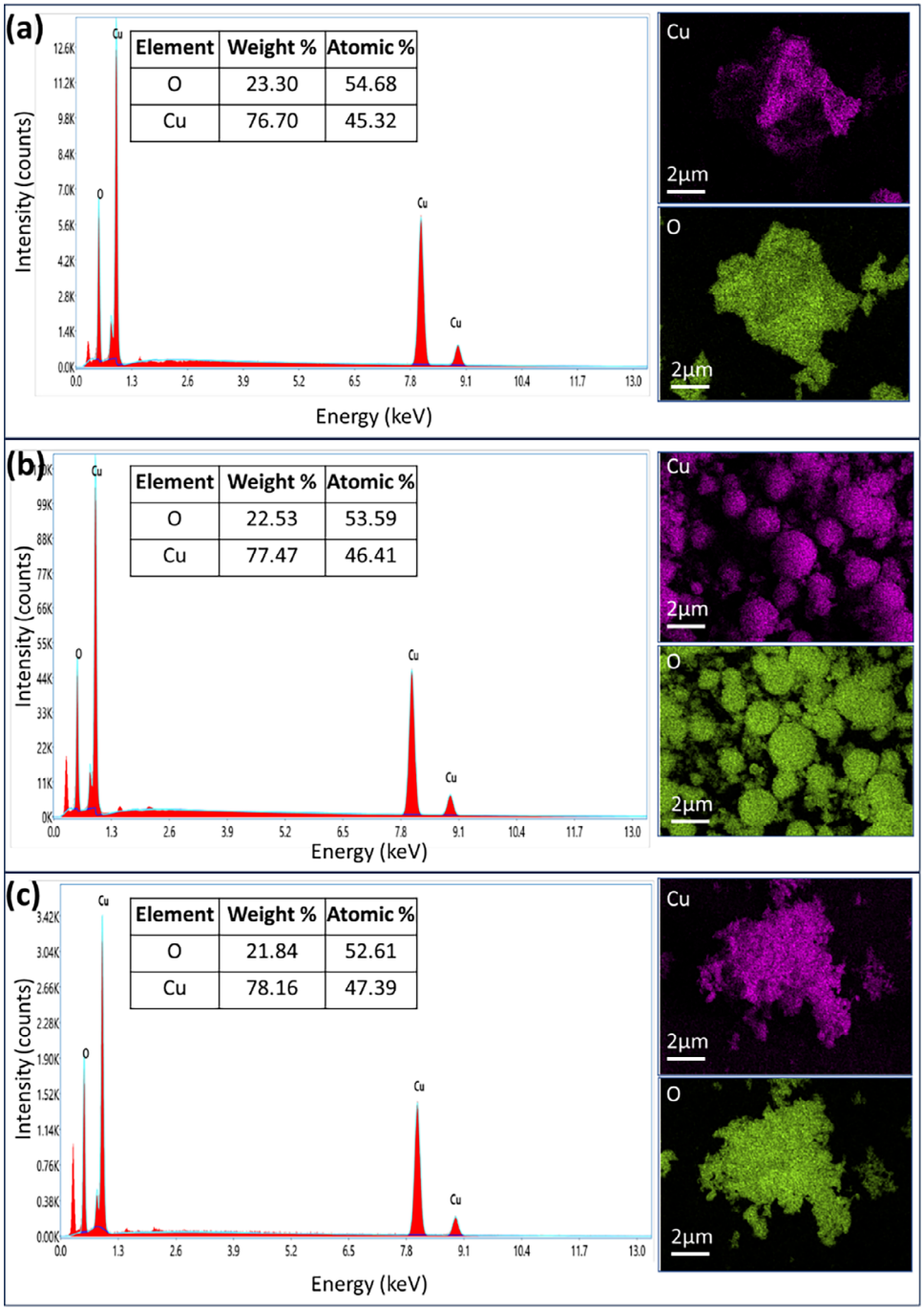

FIGURE 4 | EDX spectra of CuO nanostructures synthesized via the microwave method. (a) without a chelating agent, (b) with EDTA, and (c) PEG.

therefore, very critical in determining the elemental composition and texture of CuO nanostructures.

Figure 5a presents the UV-DRS spectrum indicates the reflectance properties of CuO nanostructures prepared without a chelating agent, with EDTA as a chelating agent, and with PEG as a stabilizing agent. All samples exhibit a sharp increase in reflectance between 800 and 900 nm, a characteristic feature of CuO nanostructures. Reflectance levels vary depending on the synthesis method, with the PEG-assisted sample (blue line) exhibiting the highest reflectance, followed by the sample without a chelating agent (black line), and then the lowest reflectance for the EDTA-assisted sample (red line). Such variation demonstrates how the choice of synthesis additives alters light interaction and consequently the optical properties of the nanostructures, which is of utmost importance in photocatalysis applications. A Tauc plot is used to determine the energy bandgap (Eg) of materials, primarily semiconductors, from UV-DRS data. The plot is derived from the equation: $(\alpha h\nu)^2 = A(h\nu - E_g)$ [38, 39]. In this expression, α is the absorption coefficient, h is Planck's constant, ν is the frequency of the incident light, Eg is the bandgap of the material, and A is a constant of proportionality. The absorption coefficient determined from the reflectance data can be used to calculate the bandgap by extrapolating the linear

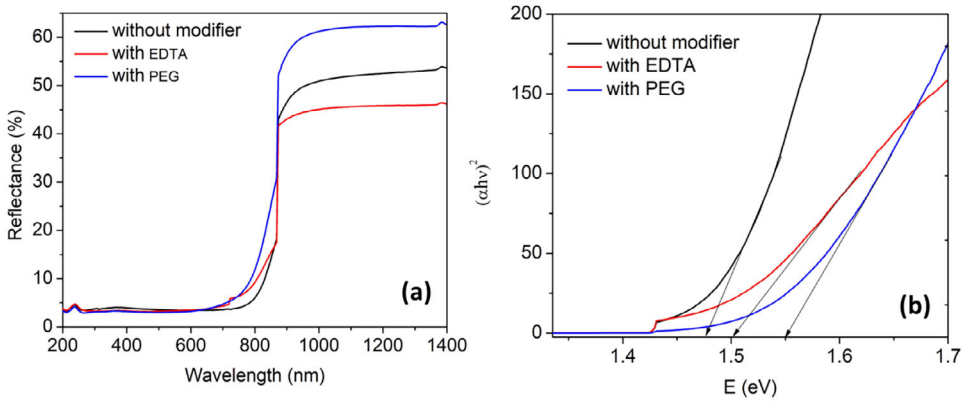

FIGURE 5 | (a) UV–vis–NIR diffuse reflectance spectra (b) Tauc plot for the estimation of the optical bandgap (Eg) of CuO nanoparticles synthesized without a modifier (black), with EDTA (red), and with PEG (blue).

portion of the hν plot to the x-axis, where absorption is zero. Figure 5b shows the Tauc plot for CuO nanostructures without the chelating agent, with EDTA, and with PEG. The calculated bandgap energies for the three samples are 1.47, 1.50, and 1.98 eV, respectively. The increase in bandgap with EDTA and PEG modifications suggests that these agents influence the structural and electronic properties of CuO, possibly due to a reduction in particle size and enhanced quantum confinement effects [11, 40]. These findings highlight the impact of chelating and stabilizing agents on the optical behavior of CuO, which is significant for applications in photocatalysis.

Photoluminescence and photocatalysis are connected in that they both involve the production of electron-hole pairs by light in a semiconductor [41]. A semiconductor with high photocatalytic activity is typically associated with low photoluminescence intensity because a large fraction of the electron-hole pairs are efficiently separated to participate in reactions (photocatalysis), and thus, a smaller fraction recombines to emit light (photoluminescence). On the other hand, strong photoluminescence is often interpreted as a higher rate of electron-hole recombination, which implies that less energy is available for photocatalysis [41]. The PL spectra of CuO nanoparticles prepared in different ways under 325 nm excitation exhibit two major emission peaks at approximately 365 and 469 nm (Figure 6). The emission detected at 365 nm confirms the occurrence of near-band-edge excitonic recombination. On the other hand, the blue emission at 469 nm is linked to the existence of intrinsic lattice defects, such as oxygen vacancies [42, 43]. Among the samples, pure CuO exhibits the highest photoluminescence intensity, indicating good crystallinity and a high number of radiative defect centers. The EDTA-assisted CuO and PEG-modified CuO exhibit the lowest photoluminescence emission compared to pure CuO, suggesting that they have non-radiative traps or structural disorder, which hinders radiative recombination. Since the lower photoluminescence intensity corresponds to less electron–hole recombination [41], the PEG-modified CuO is thought to be the most effective photocatalyst, followed by the EDTA-modified sample, while pure CuO might be the least effective because of its high recombination rate (Figure 6).

The UV–vis absorption spectra (Figure 7) show the photocatalytic degradation of eosin yellow by the prepared CuO photocatalyst.

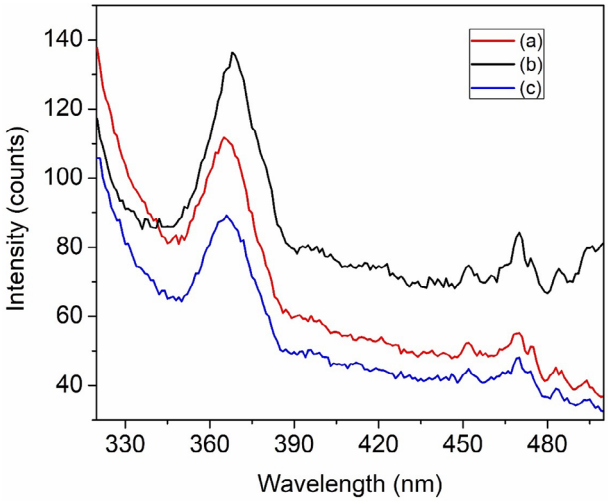

FIGURE 6 | (a) Photoluminescence spectra of CuO nanoparticles synthesized without a modifier (a), with EDTA (b), and with PEG (c).

The characteristic absorption peak of eosin yellow was 515 nm [44]. It noted that the absorption maxima of eosin yellow decreased gradually with increasing degradation time. These results clearly indicate the dye degradation efficiency of the prepared CuO photocatalyst for eosin yellow dye. Among the tested samples, the maximum degradation efficiency was exhibited by the CuO prepared with PEG, followed by the CuO prepared with EDTA, while the CuO prepared without a chelating agent showed comparatively lower activity. For PEG, this is explained by a higher bandgap and an enhanced surface area due to its rod-like shape, which further helps in charge-carrier separation, reducing the chances for recombination [45, 46]. Additionally, EDTA-assisted CuO exhibited higher photocatalytic activity compared to pure CuO, owing to better control over particle growth, which is dependent on surface properties. The results demonstrated the role of chelating agents in optimizing CuO nanostructures for dye degradation in photocatalytic applications, qualifying them as a potential candidate for wastewater treatment.

The photocatalytic degradation of eosin yellow using a prepared CuO photocatalyst was investigated. Photodegradation efficiency (Figure 8a) indicates that PEG-assisted CuO showed 98.13% degra-

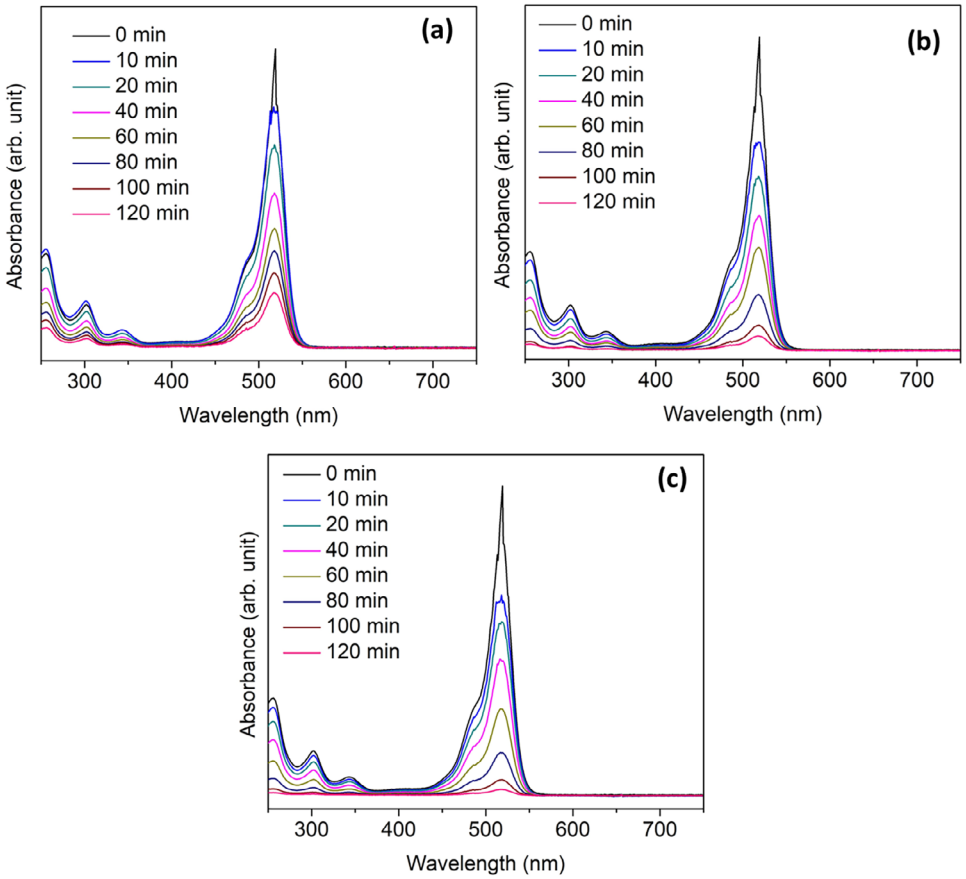

FIGURE 7 | UV–vis absorption spectra illustrate the photocatalytic degradation of Eosin Yellow using CuO photocatalysts synthesized via microwave method by (a) without a chelating agent, (b) with EDTA, and (c) with PEG.

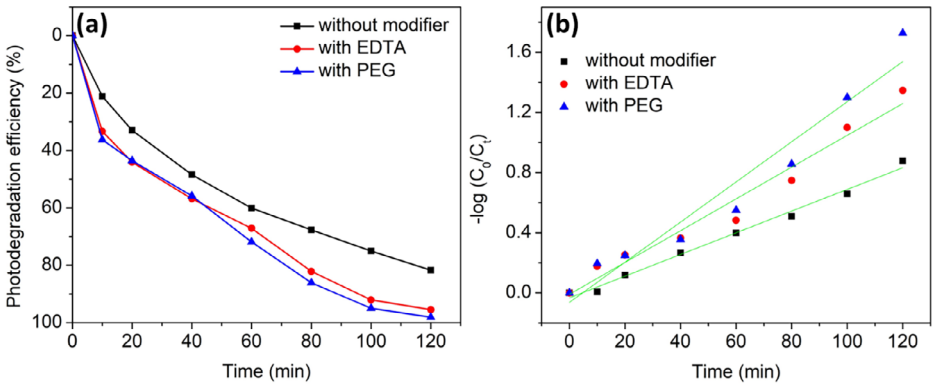

FIGURE 8 | (a) Photodegradation efficiency and (b) kinetic analysis of CuO nanostructures.

dation of dye within the 120 min of experimentation, thereby outperforming EDTA-mediated CuO (95.50%) and unmodified CuO (81.70%). Such a variation in photocatalytic performance is considered to be intensely dependent on the various morphological features resulting from different chelating agents. The CuO obtained without a chelating agent has been found to possess irregular, flaky, and plate-like structures with rough surfaces, as revealed by morphological analysis. Such structural imperfections have led to a decreased surface area and fewer photocatalytically active sites, resulting in slower degradation. In contrast, CuO modified by EDTA has created spherical nanoparticles of relatively uniform size, thereby increasing the surface area and light absorption, which leads to better photocatalytic activity compared to unmodified CuO. Moreover, PEG-modified CuO exhibited a rod-like nanostructure, which significantly enhanced its photocatalytic activity by increasing the surface area and providing more active sites for the adsorption of dyes and degradation. Furthermore, the elongated morphology enhances charge separation and transport, thus avoiding electron-hole recombination and improving overall photocatalytic efficiency. The kinetic analysis (Figure 8b) is based on the pseudo-first-order model [46, 47], which provides further evidence to support the photocatalytic activity of the samples. The rate constant (k) was highest for PEG-modified CuO (k = 0.01335 s^{-1}), followed by

TABLE 2 | Comparison between the present study and various other studies on CuO nanomaterials in terms of their precursors, synthesis processes, obtained morphologies, target pollutants, and degradation efficiencies.

Authors and references	Precursors	Synthesis method	Morphologies	Model pollutants	Degradation efficiency
Sadollahkhani et al. [48]	Copper nitrate and HMTA	Hydrothermal method	Nanorods, nanoleaves and nanosheets	Congo red	67%, 48% and 12%
Said et al. [49].	$Cu(OAc)_2{\cdot}H_2O$, NaOH, water, ethanol	Precipitation method	Nanorods and spherical NPs	Congo red	80% and 68%
Nazim et al. [50]	$CuCl_2{\cdot}2H_2O$, NaOH, oxalic acid dihydrate	Precipitation method	Porous nanosheet	Allura red	96.99%
Cansu Sazak et al. [51]	$Cu(SO_4).5H_2O$, Knautia arvensis flower extract	Green synthesis	Spherical NPs	Remazol brilliant blue R and napthol blue black	69% and 71%
Khedr et al. [52].	$Cu(OAc)_2{\cdot}H_2O$, NaOH, citrus aurantium peel extract	Microwave-assisted green synthesis	Spherical NPs	methylene blue	97.5%
Liu et al. [8]	copper nitrate trihydrate, polyethylene glycol, NaOH	Hydrothermal method	nanoribbons	Rhodamine B	92%
Rahman et al. [53].	Copper acetate, HMTA, NaOH	Hydrothermal process	Nanorods	Methylene blue	~70%
Rao et al. [54].	$CuSO_4$, PEG, NaOH	Precipitation method	Nanosheet	Methylene blue and rhodamine B	90% and 15%
Present study	Copper nitrate, polyethylene glycol, EDTA, NaOH	Microwave method	Flakes spherical NPs nanorods	Eosin yellow	81%, 95 and 98%

EDTA-modified CuO ($k = 0.01057\ s^{-1}$), and lowest for unmodified CuO ($k = 0.00722\ s^{-1}$). This trend confirms that PEG-assisted synthesis optimizes charge carrier dynamics and enhances reaction kinetics. The increase in the rate constant of PEG-modified CuO suggests that the rod-like structure is a crucial factor that accelerates photodegradation through effective electron transfer, thereby sustaining reaction rates over time. Therefore, PEG-modified CuO exhibits better photocatalytic activity and kinetics than other samples due to its rod-like structure owing to more efficient light absorption, surface reactivity, and charge transport properties.

In Table 2, we have compared the present results with those in the literature. It revealed the importance of the synthesis method, the role of the precursor, and the significance of CuO morphology on the photocatalytic activity of CuO for the photocatalytic degradation of organic pollutants. In the current work, we have introduced a microwave-assisted synthesis method utilizing copper nitrate, polyethylene glycol, EDTA, and NaOH, yielding irregular flakes, rod-like, and spherical nanoparticles with tunable degradation efficiency for eosin yellow. Our findings emphasized the significant relationship between nanostructure morphology and photocatalytic degradation efficiency. In fact, the PEG-assisted synthesis of CuO yields a well-optimized nanostructure that effectively enhances dye degradation, making it highly feasible for wastewater treatment applications.

4 | Conclusions

In this study, we investigated the microwave-assisted synthesis of morphology-controlled copper oxide nanostructures and examined the role of chelating agents in their structural, optical, and photocatalytic properties. PEG-assisted CuO developed nanorods, while EDTA-assisted CuO produced spherical nanoparticles, and unmodified CuO appeared as irregular flakes. This presented a bandgap shift from 1.47 eV (unmodified CuO) to 1.50 eV (EDTA-assisted CuO) and 1.55 eV (PEG-assisted CuO) as a result of quantum confinement effects. Photocatalytic studies revealed that the morphology of the CuO nanostructure has a significant impact on the degradation of eosin yellow, thereby affecting their photocatalytic performance. Kinetic analysis confirmed the highest degradation rate for PEG-assisted CuO ($k = 0.01335\ s^{-1}$). Hence, synthesizing CuO nanostructures with controlled morphology is a promising approach for developing highly effective photocatalysts for environmental remediation.

Author Contributions

G. Suresh Kumar: Investigation, methodology, writing. K. Lalithambigai: Data curation, review and editing, validation. S. Ranjith Priyan: Data curation, data visualization and analysis. Srinivasan Ramalingam and Raji Atchudan: Data curation, data visualization, review and editing. Mohd. Shkir: Data curation, funding acquisition, review and editing. All authors read and approved the final manuscript.

Acknowledgements

The author from PSGCAS sincerely thanks the management for their support and encouragement.

Ethical Approval

This article does not contain any studies with human participants or animals performed by any of the authors.

Conflicts of Interest

The authors declare no conflicts of interest.

Data Availability Statement

The data that support the findings of this study are available from the corresponding author upon reasonable request.

References

1. N. Baig, I. Kammakakam, and W. Falath, "Nanomaterials: A Review of Synthesis Methods, Properties, Recent Progress, and Challenges," *Materials Advances* 2 (2021): 1821–1871, https://doi.org/10.1039/D0MA00807A.

2. R. A. Much, K. Winkelmann, and M. Hugerat, *Nanochemistry for Chemistry Educators* (The Royal Society of Chemistry, 2022), https://doi.org/10.1039/9781839164774.

3. B. Mekuye and B. Abera, "Nanomaterials: An Overview of Synthesis, Classification, Characterization, and Applications," *Nano Select* 4 (2023): 486–501, https://doi.org/10.1002/nano.202300038.

4. Q. Zhang, K. Zhang, D. Xu, et al., "CuO Nanostructures: Synthesis, Characterization, Growth Mechanisms, Fundamental Properties, and Applications," *Progress in Materials Science* 60 (2014): 208–337, https://doi.org/10.1016/j.pmatsci.2013.09.003.

5. P. Raizada, A. Sudhaik, S. Patial, et al., "Engineering Nanostructures of CuO-Based Photocatalysts for Water Treatment: Current Progress and Future Challenges," *Arabian Journal of Chemistry* 13 (2020): 8424–8457, https://doi.org/10.1016/j.arabjc.2020.06.031.

6. A. S. Zoolfakar, R. A. Rani, A. J. Morfa, A. P. O'Mullane, and K. Kalantar-zadeh, "Nanostructured Copper Oxide Semiconductors: A Perspective on Materials, Synthesis Methods and Applications," *Journal of Materials Chemistry C* 2 (2014): 5247–5270, https://doi.org/10.1039/C4TC00345D.

7. K. Dulta, G. Koşarsoy Ağçeli, P. Chauhan, R. Jasrotia, P. K. Chauhan, and J. O. Ighalo, "Multifunctional CuO Nanoparticles with Enhanced Photocatalytic Dye Degradation and Antibacterial Activity," *Sustainable Environment Research* 32 (2022): 2, https://doi.org/10.1186/s42834-021-00111-w.

8. J. Liu, J. Jin, Z. Deng, et al., "Tailoring CuO Nanostructures for Enhanced Photocatalytic Property," *Journal of Colloid and Interface Science* 384 (2012): 1–9, https://doi.org/10.1016/j.jcis.2012.06.044.

9. M. B. Gawande, S. N. Shelke, R. Zboril, and R. S. Varma, "Microwave-Assisted Chemistry: Synthetic Applications for Rapid Assembly of Nanomaterials and Organics," *Accounts of Chemical Research* 47, no. 4 (2014): 1338–1348, https://doi.org/10.1021/ar400309b.

10. A. Kumar, Y. Kuang, Z. Liang, and X. Sun, "Microwave Chemistry, Recent Advancements, and Eco-friendly Microwave-Assisted Synthesis of Nanoarchitectures and Their Applications: A Review," *Materials Today Nano* 11 (2020): 100076, https://doi.org/10.1016/j.mtnano.2020.100076.

11. J. Duraimurugan, G. S. Kumar, M. Venkatesh, P. Maadeswaran, and E. K. Girija, "Morphology and Size Controlled Synthesis of Zinc Oxide Nanostructures and Their Optical Properties," *Journal of Materials Science: Materials in Electronics* 29 (2018): 9339–9346, https://doi.org/10.1007/s10854-018-8964-9.

12. W.-W. Wang, Y.-J. Zhu, G.-F. Cheng, and Y.-H. Huang, "Microwave-assisted Synthesis of Cupric Oxide Nanosheets and Nanowhiskers," *Materials Letters* 60 (2006): 609–612, https://doi.org/10.1016/j.matlet.2005.09.056.

13. A. Roy, A. Sharma, S. Yadav, L. T. Jule, and R. Krishnaraj, "Nanomaterials for Remediation of Environmental Pollutants," *Bioinorganic*

Chemistry and Applications 2021 (2021): 1–20, https://doi.org/10.1155/2021/1764647.

14. B. J. Singh, A. Chakraborty, and R. Sehgal, "A Systematic Review of Industrial Wastewater Management: Evaluating Challenges and Enablers," *Journal of Environmental Management* 348 (2023): 119230, https://doi.org/10.1016/j.jenvman.2023.119230.

15. A. S. Adday and S. M. Al-Jubouri, "Developing a Versatile Visible-Light-Driven Polyvinylidene Fluoride/Ag2O@CRA Photocatalytic Membrane for Efficient Treatment of Organic Pollutants-Contained Wastewater," *Journal of Water Process Engineering* 73 (2025): 107713, https://doi.org/10.1016/j.jwpe.2025.107713.

16. M. A. Al-Nuaim, A. A. Alwasiti, and Z. Y. Shnain, "The Photocatalytic Process in the Treatment of Polluted Water," *Chemical Papers* 77 (2023): 677–701, https://doi.org/10.1007/s11696-022-02468-7.

17. F. Mohamadpour and A. M. Amani, "Photocatalytic Systems: Reactions, Mechanism, and Applications," *RSC Advances* 14 (2024): 20609–20645, https://doi.org/10.1039/D4RA03259D.

18. A. S. Adday and S. M. Al-Jubouri, "Photocatalytic Oxidative Removal of the Organic Pollutant From Wastewater Using Recyclable Ag_2O@CRA Heterojunction Photocatalyst," *Case Studies in Chemical and Environmental Engineering* 10 (2024): 100852, https://doi.org/10.1016/j.cscee.2024.100852.

19. N. Dasineh Khiavi, R. Katal, S. Kholghi Eshkalak, S. Masudy-Panah, S. Ramakrishna, and H. Jiangyong, "Visible Light Driven Heterojunction Photocatalyst of CuO–Cu_2O Thin Films for Photocatalytic Degradation of Organic Pollutants," *Nanomaterials* 9, no. 7 (2019): 1011, https://doi.org/10.3390/nano9071011.

20. P. Vomáčka, V. Štengl, J. Henych, and M. Kormunda, "Shape-Controlled Synthesis of Sn-Doped CuO Nanoparticles for Catalytic Degradation of Rhodamine B," *Journal of Colloid & Interface Science* 481 (2016): 28–38, https://doi.org/10.1016/j.jcis.2016.07.026.

21. T. P. Vijayakumar, M. D. Benoy, J. Duraimurugan, et al., "Effect of G-C_3N_4 on Structural, Optical, and Photocatalytic Properties of Hexagonal Cylinder-Like Twinned ZnO Microcrystals Prepared by the Hydrothermal Method," *Journal of Materials Science: Materials in Electronics* 32 (2021): 24095–24106, https://doi.org/10.1007/s10854-021-06872-9.

22. T. P. Vijayakumar, M. D. Benoy, J. Duraimurugan, et al., "Hydrothermal Synthesis of CuO/G-C3N4 Nanosheets for Visible-Light Driven Photodegradation of Methylene Blue," *Diamond and Related Materials* 121 (2022): 108735, https://doi.org/10.1016/j.diamond.2021.108735.

23. L. Guo, F. Tong, H. Liu, H. Yang, and J. Li, "Shape-Controlled Synthesis of Self-assembly Cubic CuO Nanostructures by Microwave," *Materials Letters* 71 (2012): 32–35, https://doi.org/10.1016/j.matlet.2011.11.105.

24. Y.-J. Zhu and F. Chen, "Microwave-Assisted Preparation of Inorganic Nanostructures in Liquid Phase," *Chemical Reviews* 114, no. 12 (2014): 6462–6555, https://doi.org/10.1021/cr400366s.

25. S. M. Derayea and D. M. Nagy, "Application of a Xanthene Dye, Eosin Y, as Spectroscopic Probe in Chemical and Pharmaceutical Analysis; A Review," *Reviews in Analytical Chemistry* 37 (2018): 20170020, https://doi.org/10.1515/revac-2017-0020.

26. M. C. Shibu, M. D. Benoy, G. S. Kumar, et al., "Hydrothermal-Assisted Synthesis and Characterization of MWCNT/Copper Oxide Nanocomposite for the Photodegradation of Methyl Orange under Direct Sunlight," *Diamond and Related Materials* 134 (2023): 109778, https://doi.org/10.1016/j.diamond.2023.109778.

27. J. Madona, C. Sridevi, G. Velraj, A. Dhayal Raj, and A. George, "Surfactant Assisted Morphology Controlled CuO Nanostructures for Enhanced Photocatalytic Performance and Bacterial Growth Inhibition," *Materials Science and Engineering: B* 294 (2023): 116562, https://doi.org/10.1016/j.mseb.2023.116562.

28. B. Lefez, R. Souchet, K. Kartouni, and M. Lenglet, "Infrared Reflection Study of CuO in Thin Oxide Films," *Thin Solid Films* 268 (1995): 45–48, https://doi.org/10.1016/0040-6090(95)06872-4.

29. H. Wang, J. Z. Xu, J. J. Zhu, and H. Y. Chen, "Preparation of CuO Nanoparticles by Microwave Irradiation," *Journal of Crystal Growth* 244 (2002): 88–94, https://doi.org/10.1016/S0022-0248(02)01571-3.

30. R. Javed, M. Ahmed, I. Haq, S. Nisa, and M. Zia, "PVP and PEG doped CuO nanoparticles are more biologically active: Antibacterial, antioxidant, antidiabetic and cytotoxic perspective", *Materials Science and Engineering: C*, 79 (2017):108–115, https://doi.org/10.1016/j.msec.2017.05.006.

31. B. Smith, *Infrared Spectral Interpretation* (CRC Press, 2018), https://doi.org/10.1201/9780203750841.

32. K. Giannousi, E. Hatzivassiliou, S. Mourdikoudis, G. Vourlias, A. Pantazaki, and C. Dendrinou-Samara, "Synthesis and biological evaluation of PEGylated CuO nanoparticles", *Journal of Inorganic Biochemistry*, 164, (2016): 82–90, https://doi.org/10.1016/j.jinorgbio.2016.09.003.

33. J. Jayaprakash, N. Srinivasan, and P. Chandrasekaran, "Surface Modifications of CuO Nanoparticles Using Ethylene Diamine Tetra Acetic Acid as a Capping Agent by Sol–gel Routine," *Spectrochimica Acta Part A: Molecular and Biomolecular Spectroscopy* 123 (2014): 363–368, https://doi.org/10.1016/j.saa.2013.12.080.

34. K. Giannousi, E. Hatzivassiliou, S. Mourdikoudis, G. Vourlias, A. Pantazaki, and C. Dendrinou-Samara, "Synthesis and Biological Evaluation of PEGylated CuO Nanoparticles," *Journal of Inorganic Biochemistry* 164 (2016): 82–90, https://doi.org/10.1016/j.jinorgbio.2016.09.003.

35. D. P. Singh, A. K. Ojha, and O. N. Srivastava, "Synthesis of Different $Cu(OH)_2$ and CuO (Nanowires, Rectangles, Seed-, Belt-, and Sheetlike) Nanostructures by Simple Wet Chemical Route," *The Journal of Physical Chemistry C* 113, no. 9 (2009): 3409–3418, https://doi.org/10.1021/jp804832g.

36. S. D. Bajaj, P. V. Tekade, G. V. Lakhotiya, and P. G. Borkar, "Microwave Assisted Fast Synthesis of CuO Nanoflakes: Catalytic Application in the Synthesis of 1,4-Dihydropyridine," *Acta Physica Polonica A* 132 (2017): 1294, https://doi.org/10.12693/APhysPolA.132.1294.

37. H. Chen, G. Zhao, and Y. Liu, "Low-Temperature Solution Synthesis of CuO Nanorods with Thin Diameter," *Materials Letters* 93 (2013): 60–63, https://doi.org/10.1016/j.matlet.2012.11.055.

38. J. Tauc, R. Grigorovici, and A. Vancu, "Optical Properties and Electronic Structure of Amorphous Germanium," *Physica Status Solidi (b)* 15, no. 2 (1966): 627–637, https://doi.org/10.1002/pssb.19660150224.

39. P. Makuła, M. Pacia, and W. Macyk, "How to Correctly Determine the Band Gap Energy of Modified Semiconductor Photocatalysts Based on UV–Vis Spectra," *Journal of Physical Chemistry Letters* 9, no. 23 (2018): 6814–6817, https://doi.org/10.1021/acs.jpclett.8b02892.

40. H. K. Mallick, Y. Zhang, J. Pradhan, M. P. K. Sahoo, and A. K. Pattanaik, "Influence of Particle Size and Defects on the Optical, Magnetic and Electronic Properties of Al Doped SnO2 Nanoparticles," *Journal of Alloys and Compounds* 854 (2021): 156067, https://doi.org/10.1016/j.jallcom.2020.156067.

41. T. K. Le, M. Kang, V. T. Tran, and S. W. Kim, "Relation of Photoluminescence and Sunlight Photocatalytic Activities of Pure V_2O_5 Nanohollows and V_2O_5/RGO Nanocomposites," *Materials Science in Semiconductor Processing* 100 (2019): 159–166, https://doi.org/10.1016/j.mssp.2019.04.047.

42. X. Zhao, P. Wang, Z. Yan, and N. Ren, "Room Temperature Photoluminescence Properties of CuO Nanowire Arrays," *Optical Materials* 42 (2015): 544–547, https://doi.org/10.1016/j.optmat.2014.12.032.

43. A. R. Ansari, A. H. Hammad, M. S. Abdel-wahab, M. Shariq, and M. Imran, "Structural, Optical and Photoluminescence Investigations of Nanocrystalline CuO Thin Films at Different Microwave Powers," *Optical and Quantum Electronics* 52 (2020): 426, https://doi.org/10.1007/s11082-020-02535-x.

44. V. J. Mayani, S. V. Mayani, and S. W. Kim, "A Sustainable Nanocomposite Au(Salen)@CC for Catalytic Degradation of Eosin Y and Chromotrope 2R Dyes," *Scientific Reports* 7 (2017): 7239, https://doi.org/10.1038/s41598-017-07707-6.

45. A. Chawla, A. Sudhaik, R. K. Sonu, et al., "Recent Advances in Synthesis Methods and Surface Structure Manipulating Strategies of Copper Selenide (CuSe) Nanoparticles for Photocatalytic Environmental and Energy Applications," *Journal of Environmental Chemical Engineering* 12 (2024): 113125, https://doi.org/10.1016/j.jece.2024.113125.

46. C. Jayakrishnan, S. R. Sheeja, G. S. Kumar, K. Lalithambigai, J. Duraimurugan, and M. M. Alam, "Hydrothermal Assisted Synthesis of Shape-Controlled Zinc Oxide Nanostructures for Tuneable Photodegradation of Methylene Blue Pollutant," *Journal of Sol-Gel Science and Technology* 112 (2024): 262–276, https://doi.org/10.1007/s10971-024-06515-5.

47. E. D. Revellame, D. L. Fortela, W. Sharp, R. Hernandez, and M. E. Zappi, "Adsorption Kinetic Modeling Using Pseudo-First Order and Pseudo-Second Order Rate Laws: A Review," *Cleaner Engineering and Technology* 1 (2020): 100032, https://doi.org/10.1016/j.clet.2020.100032.

48. A. Sadollahkhani, Z. Hussain Ibupoto, S. Elhag, O. Nur, and M. Willander, "Photocatalytic Properties of Different Morphologies of CuO for the Degradation of Congo Red Organic Dye," *Ceramics International* 40 (2014): 11311–11317, https://doi.org/10.1016/j.ceramint.2014.03.132.

49. M. I. Said, A. A. Othman, and E. M. Abd elhakeem, "Structural, Optical and Photocatalytic Properties of Mesoporous CuO Nanoparticles with Tunable Size and Different Morphologies," *RSC Advances* 11 (2021): 37801–37813, https://doi.org/10.1039/D1RA04780A.

50. M. Nazim, A. A. P. Khan, A. M. Asiri, and J. H. Kim, "Exploring Rapid Photocatalytic Degradation of Organic Pollutants with Porous CuO Nanosheets: Synthesis, Dye Removal, and Kinetic Studies at Room Temperature," *ACS Omega* 6, no. 4 (2021): 2601–2612, https://doi.org/10.1021/acsomega.0c04747.

51. C. Sazak, A. Attar, S. Ari Yuka, and M. A. Yapaoz, "Bio-Capped Multifunctional CuO Nanoparticles via Knautia Arvensis for Dye Removal, Antibacterial and Antifungal Efficiency, and Molecular Docking," *Materials Research Express* 11 (2024): 055008, https://doi.org/10.1088/2053-1591/ad4c3a.

52. A. I. Khedr and M. H. H. Ali, "Eco-Friendly Fabrication of Copper Oxide Nanoparticles Using Peel Extract of *Citrus Aurantium* for the Efficient Degradation of Methylene Blue Dye," *Scientific Reports* 14 (2024): 29156, https://doi.org/10.1038/s41598-024-79589-4.

53. Q. I. Rahman, A. Ali, N. Ahmad, M. B. Lohani, S. K. Mehta, and M. Muddassir, "Synthesis and Characterization of CuO Rods for Enhanced Visible Light Driven Dye Degradation," *Journal of Nanoscience and Nanotechnology* 20, no. 12 (2020): 7716–7723, https://doi.org/10.1166/jnn.2020.18713.

54. M. P. Rao, P. Sathishkumar, R. V. Mangalaraja, A. M. Asiri, P. Sivashanmugam, and S. Anandan, "Simple and Low-Cost Synthesis of CuO Nanosheets for Visible-Light-Driven Photocatalytic Degradation of Textile Dyes," *Journal of Environmental Chemical Engineering* 6, no. 2 (2018): 2003–2010, https://doi.org/10.1016/j.jece.2018.03.008.